

Towards a Practical Implementation of Coherent WDM: Analytical, Numerical and Experimental studies

S. K. Ibrahim, (*IEEE Member*), J. Zhao, F. C. Garcia Gunning, (*IEEE Member*), P. Frascella, (*IEEE Student Member*), F. H. Peters, A. D. Ellis

Department of Physics and Tyndall National Institute, University College Cork, Ireland

Corresponding author: selwan.ibrahim@tyndall.ie

Abstract: Future optical networks will require the implementation of very high capacity (and therefore spectral efficient) technologies. Multi-carrier systems, such as Orthogonal Frequency Division Multiplexing (OFDM) and Coherent WDM (CoWDM) are promising candidates. In this paper we present analytical, numerical and experimental investigations of the impact of the relative phases between optical subcarriers of CoWDM systems, and the effect that the number of independently modulated subcarriers can have to the performance. We numerically demonstrate a 5-subcarrier and 3-subcarrier 10Gbaud CoWDM system with direct detected ASK and differentially/coherently detected (D)PSK. The simulation results are compared to experimental measurements of a 32Gbit/s DPSK CoWDM system in two configurations. The first configuration was a practical 3-modulator array where all 3 subcarriers were independently modulated, the second configuration being a traditional 2-modulator odd/even configuration, where only odd and even subcarriers were independently modulated. Simulation and experimental results both indicate that the independent modulation implementation has a greater dependency on the relative phases between subcarriers, with a stronger penalty for the center subcarrier, than the odd/even modulation scheme.

Index Terms: Optical fiber communication, Optical modulation, Phase modulation

1. Introduction

The rapid growth in video-based Internet applications is driving the demand for higher speed optical transmission systems for the access, metro-core, and long haul networks, which requires bandwidth efficient telecommunications systems. One promising approach is the use of optical multi-carrier spectrally efficient transmission techniques, where the subcarrier spacing is equal to its symbol rate [1-20]. This was demonstrated by optically generated Orthogonal Frequency Division Multiplexing (all-optical OFDM) [2-8], optically generated Coherent Wavelength Division Multiplexing (CoWDM) [9-13], traditional electrically generated OFDM [14-15], and also combining all-optical and traditional electrical OFDM techniques resulting in multi-banded electro-optical OFDM [16-19]. All-optical implementations of OFDM/CoWDM offer the prospect of high aggregate capacity and spectral efficiency, with impairment tolerances scaling with the symbol rate of each subcarrier. However, the majority of earlier reports of such techniques tended to use only two modulators in an odd/even configuration. This configuration does not address the practical implementation penalties arising from the fact that neighboring subcarriers carry different data patterns with overlapping spectra [11-13].

Typically, in all-optical OFDM systems, unless ideal matched filters are deployed [7-8], non-ideal filters result in residual inter-channel crosstalk at the receiver-side, whose influence on system performance is related to the relative phases between the subcarriers. This impact can be mitigated by increasing the guard band interval [6], reducing the number of interfering channels

1 through polarization interleaving [3] or by using lower number of subcarriers [4], restoring the
 2 channel orthogonality at the transmitter through electronic pre-compensation [20, 21], or via phase
 3 control for each subcarrier, resulting in the reduction of signal-crosstalk beating at the decision
 4 point (CoWDM) [9-13]. CoWDM also offers the advantage of using low cost receiver filters with out
 5 the need for expensive and power hungry DSP based receivers.

6 In this paper we examine the use of phase control in the transmitter to control the crosstalk arising
 7 from the neighbor interfering optical subcarriers due to the partially overlapping spectra with the
 8 targeted subcarrier at the transmitter. It is important to study this effect because, in practical
 9 realizations, the phase between the subcarriers may vary due to any random environment changes,
 10 such as temperature, that would cause random length changes resulting in random phase
 11 variations. We present, for the first time, an analytical theory of the residual crosstalk penalty,
 12 which is verified by direct numerical simulations of CoWDM with Amplitude Shift Keying (ASK),
 13 Differential Phase Shift Keying (DPSK), and Binary Phase Shift Keying (BPSK) modulation formats.
 14 Moreover, we experimentally verify the predicted impact of the nearest neighbor crosstalk in a 3-
 15 subcarrier 32Gbit/s DPSK CoWDM system.

16 The paper is organized as follows. In section 2, we present an analytical theory of the phase
 17 relationship between subcarriers on CoWDM systems. This analysis is further investigated by
 18 numerical simulations in section 3, which demonstrate a 5-subcarrier and 3-subcarrier 10Gbaud
 19 CoWDM system with direct detected ASK, and differentially (coherently) detected DPSK (BPSK) to
 20 illustrate the phase and filter bandwidth effects on the performance of these systems. In section 4,
 21 the theory and numerical simulations are confirmed by direct experimental observations for a 3-
 22 subcarrier 32Gbit/s DPSK CoWDM system using a 3-modulator independently modulated array
 23 configuration consisting of 3 independently modulated subcarriers, and an odd/even modulated
 24 configuration using only 2 modulators instead. Finally, section 5 will conclude the results.

25 2. Analytical Theory

26 Figure 1 shows a general schematic of a multi-carrier CoWDM system where the subcarriers are
 27 optically multiplexed at the transmitter side (left) and optically demultiplexed and demodulated at
 28 the receiver side (right).

29 In order to analyze the optical field $E_k^0(t)$ of any k WDM channel with a symbol period T and field
 30 amplitude E_0 , we assume a complex logical data for the n^{th} bit of the k^{th} channel ($D_{k,n}$), a pulse
 31 shape $h_{Tx}(t)$ with relative delay τ_k , and an optical carrier with frequency ω_k and phase ϕ_k :

$$32 \quad E_k^0(t) = \sum_{n=-\infty}^{+\infty} D_{k,n} E_0 h_{Tx}(t - \tau_k - nT) e^{i(\omega_k t + \phi_k)} \quad (1)$$

33 Note that $h_{Tx}(t)$ represents the optical pulse shape after modulation and, thus, it is the overall
 34 system response at the transmitter including pulse shape of the logic data, impulse response of the
 35 electrical filter, transfer function of modulation, and the impulse response of any optical filter
 36 deployed within the transmitter. In practice, $h_{Tx}(t)$ is usually the same for all subcarriers. Assuming
 37 that the targeted subcarrier j is optically demultiplexed using a receiver-side filter with a frequency
 38 response $H_{Rx,j}(\omega)$, the spectrum of the optical field after filtering can be represented as:

$$39 \quad \varepsilon_j'(\omega) = \sum_{k=1}^J \sum_{n=-\infty}^{+\infty} D_{k,n} E_0 e^{i\phi_k} H_{Tx}(\omega - \omega_k) e^{-i(\tau_k + nT)(\omega - \omega_k)} H_{Rx,j}(\omega) \quad (2)$$

40 where J is the number of subcarriers, and $H_{Tx}(\omega)$ is the equivalent frequency response
 41 corresponding to the transmitter impulse response $h_{Tx}(t)$. The time-domain signal after channel
 42 demultiplexing for the subcarrier j is obtained by taking the inverse Fourier transform of (2):

$$43 \quad E_j'(t) = E_0 \sum_{k=1}^J \sum_{n=-\infty}^{\infty} S_{k,n} I_{k,j}(t - \tau_k - nT) e^{i\omega_j t + i(\omega_k - \omega_j)(nT + \tau_k)} \quad (3)$$

1 where $S_{k,n} = D_{k,n} e^{i\phi_k}$ represents the complex logical data, including the subcarrier phase, and

$$2 \quad I_{k,j}(t) = \frac{1}{2\pi} \int_{-\infty}^{+\infty} H_{Tx}(\omega - \omega_k + \omega_j) H_{Rx,j}(\omega + \omega_j) e^{i\omega t} d\omega \quad (4)$$

3 is the baseband representation of the signal pulse shape for the k^{th} channel after optical filtering by
4 the demultiplexing filter targeted to the subcarrier j .

5 For an orthogonal multi-carrier system, we assume that all subcarriers are temporally aligned with
6 a zero delay, i.e. $\tau_k=0$, and that the channel spacing satisfies the orthogonality condition
7 $\omega_k - \omega_j = 2\pi \cdot r/T$, where r is an integer. Note that, unless the carrier phase ϕ_k is constant, the
8 orthogonality condition is only approximately satisfied, since any time variation in phase may also
9 be expressed as a change in carrier frequency.

10 In order to determine the detected electrical signal $V_j(t)$, one must first identify the detection method.
11 In direct-detected systems $V_j(t)$ is given by:

$$12 \quad V_j(t) \propto \left| E_0 \sum_{k=1}^J \sum_{n=-\infty}^{\infty} S_{k,n} I_{k,j}(t-nT) \right|^2 \quad (5)$$

13 While in homodyne coherent-detected system, i.e. when $\omega_0 = \omega_j$, $V_j(t)$ is then given by:

$$14 \quad \begin{aligned} V_{j,\text{in-phase}}(t) &\propto \text{Re} \left\{ E_0 \sum_{k=1}^J \sum_{n=-\infty}^{\infty} S_{k,n} I_{k,j}(t-nT) e^{-i\phi_0} \right\} \\ V_{j,\text{quadrature}}(t) &\propto \text{Im} \left\{ E_0 \sum_{k=1}^J \sum_{n=-\infty}^{\infty} S_{k,n} I_{k,j}(t-nT) e^{-i\phi_0} \right\} \end{aligned} \quad (6)$$

15 where $I_{k,j}(t)$ should be interpreted in a more generic form, taking into consideration the effect of
16 receiver-side electrical filter, which may also be implemented digitally [5,16]:

$$17 \quad I_{k,j}(t) = \frac{1}{2\pi} \int_{-\infty}^{+\infty} H_{Tx}(\omega - \frac{2\pi r}{T}) H_{Rx,j}(\omega + \omega_j) H_{ele,j}(\omega) e^{i\omega t} d\omega \quad (7)$$

18 We may observe from Eq. (3) that, if $I_{k,j}(t)=0$ at the sampling instant for any $k \neq j$, the system is
19 crosstalk free. Possible conditions for crosstalk free operation (i.e. using matched filters at the
20 receiver) may include a receiver filter with a $\text{sinc}(\omega T/2)$ frequency profile coupled with ideal
21 rectangular temporal pulses from the transmitter [1], or a receiver filter with rectangular frequency
22 responses coupled with transmitted pulse trains with rectangular spectra [21]. Low crosstalk has
23 also been observed using practical bandwidth limited transmitters and filters by performing optical
24 Fourier transform at the receiver [7-8].

25

26 **2.1 Direct Detection for ASK signals**

27 In the case of direct detection for ASK signals, Eq. (5) may be expanded in order to give terms
28 related to the targeted signal level, intersymbol interference and crosstalk, when the sampling
29 instant for the m^{th} sample is mT :

$$30 \quad \begin{aligned} V_j(mT) &\propto (D_{j,m} I_{j,j}(0) e^{i\phi_j} + \sum_{n \neq m} D_{j,n} I_{j,j}((m-n)T) e^{i\phi_j} + \sum_{k \neq j} \sum_n D_{k,n} I_{k,j}((m-n)T) e^{i\phi_k}) \\ &\quad \cdot (D_{j,m}^* I_{j,j}^*(0) e^{-i\phi_j} + \sum_{q \neq m} D_{j,q}^* I_{j,j}^*((m-q)T) e^{-i\phi_j} + \sum_{p \neq j} \sum_q D_{p,q}^* I_{p,j}^*((m-q)T) e^{-i\phi_k}) \end{aligned} \quad (8)$$

31 By making a reasonable assumption that the crosstalk is dominated by the nearest neighbor
32 subcarriers, i.e. $D_{j,m}$ is only degraded by $D_{j-1,m}$ and $D_{j+1,m}$, and, for simplicity, neglecting intersymbol
33 interference, one can expand the multiplication in Eq. (8) giving:

$$\begin{aligned}
V_j(mT) \propto & \left| D_{j,m} I_{j,j}(0) \right|^2 + \left| D_{j-1,m} \cdot I_{j-1,j}(0) \right|^2 + \left| D_{j+1,m} \cdot I_{j+1,j}(0) \right|^2 \\
& + 2D_{j,m} D_{j-1,m} \cdot I_{j-1,j}(0) I_{j,j}(0) \cdot \text{Cos}(\phi_j - \phi_{j-1}) \\
& + 2D_{j,m} D_{j+1,m} \cdot I_{j+1,j}(0) I_{j,j}(0) \cdot \text{Cos}(\phi_j - \phi_{j+1}) \\
& + 2D_{j-1,m} D_{j+1,m} \cdot I_{j-1,j}(0) I_{j+1,j}(0) \cdot \text{Cos}(\phi_{j-1} - \phi_{j+1})
\end{aligned} \tag{9}$$

Here it was also assumed that the data sequences are in a single quadrature and, without loss of generality, are along the real axis.

Finally, we define a signal to crosstalk ratio (SXR) as the minimum difference between the signal levels '0' and '1' in the absence of crosstalk, divided by the sum of the maximum crosstalk levels on '1' and '0', taking the worst case data pattern of the adjacent subcarriers. Here it becomes:

$$SXR = \min_{D_{k,n}} \left(\frac{\text{intensity for '1' - intensity for '0'}}{|\text{Crosstalk in '1' level}| + |\text{Crosstalk in '0' level}|} \right) \tag{10}$$

The value of SXR and the associated worst case data pattern of the adjacent subcarriers depend on the phases of the adjacent subcarrier. However, for arbitrary phase, we can obtain a lower bound for the SXR:

$$\text{Min}(SXR_{dd}) = \frac{|I_{j,j}(0)|^2}{2|I_{j-1,j}(0)|^2 + 2|I_{j+1,j}(0)|^2 + 2|I_{j-1,j}(0)I_{j,j}(0)\cos(\phi_j - \phi_{j-1})| + 2|I_{j+1,j}(0)I_{j,j}(0)\cos(\phi_j - \phi_{j+1})| + 4|I_{j-1,j}(0)I_{j+1,j}(0)\cos(\phi_{j-1} - \phi_{j+1})|} \tag{11}$$

If the phases of CoWDM subcarriers are controlled to be $\phi_j = \phi_0 + j\pi/2$, the signal-crosstalk beating terms can be eliminated no matter what the logic data of $(j-1)^{\text{th}}$, j^{th} , and $(j+1)^{\text{th}}$ carriers is. Consequently, the sampled value is determined only by the signal level and the crosstalk-crosstalk beating. That is, the interference signal between the two nearest neighbors resulting in the SXR value low-bounded by:

$$\text{Min}(SXR_{dd})_{\phi_j = \phi_0 + j\pi/2} = \frac{|I_{j,j}(0)|^2}{2|I_{j-1,j}(0)|^2 + 2|I_{j+1,j}(0)|^2 + 4|I_{j-1,j}(0)I_{j+1,j}(0)|} \tag{12}$$

If further assumption is made that the neighboring subcarriers $(j-1)$ and $(j+1)$ carry the same data logic i.e. $D_{j-1,m} = D_{j+1,m}$, and $I_{j-1,j}(0) = I_{j+1,j}(0)$, the crosstalk terms in Eq. (9) can be fully eliminated at an appropriate phase. This case occurs for multi-carrier configurations using 2 modulators for odd/even subcarriers modulation.

2.2 Differential Direct Detection for BPSK signals

If differential detection is assumed for DPSK signals, the received electrical signals from the constructive (+) and destructive (-) paths can be given by:

$$V_j^\pm(t) \propto \left| \sum_{k=1}^J \sum_{n=-\infty}^{\infty} (S_{k,n} I_{k,j}(t-nT) e^{i\omega_j t + i(\frac{2\pi}{T})(nT)} \pm S_{k,n} I_{k,j}(t-(n-1)T) e^{i\omega_j(t+T) + i(\frac{2\pi}{T})(nT)}) \right|^2 \tag{13}$$

Therefore, the sampled value for the m^{th} bit is:

$$V_j^\pm(mT) \propto \left| \sum_{k=1}^J \sum_{n=-\infty}^{\infty} (D_{k,n} + D_{k,n+1} e^{+i\omega_j T}) I_{k,j}(t-nT) e^{i\omega_j t + i\phi_k} \right|^2 \tag{14}$$

1 In order to facilitate the derivation, we define new variables representing the decoded data from the
 2 constructive and destructive paths in terms of the transmitted (pre-coded) symbols:

$$3 \quad D_{k,n}^{\pm} = D_{k,n} \pm D_{k,n+1} e^{i\omega_k T} \quad (15)$$

4 Similar to direct detection, $I_{j,j}(t)$, the pulse shape of the j^{th} subcarrier after its optical band-pass
 5 filtering (OBPF) (before demodulation), is assumed to be intersymbol interference (ISI) free. It is
 6 also assumed that the crosstalk of the j^{th} subcarrier is generated by the nearest neighbours ($k=j\pm 1$).
 7 Therefore, one can derive V_j^{\pm} as:

$$8 \quad V_j^{\pm}(mT) \propto \left(|D_{j,m}^{\pm} I_{j,j}(0)|^2 + |D_{j-1,m}^{\pm} \cdot I_{j-1,j}(0)|^2 + |D_{j+1,m}^{\pm} \cdot I_{j+1,j}(0)|^2 \right. \\
 + 2 \operatorname{Re} \{ D_{j,m}^{\pm} \cdot D_{j-1,m}^{\pm} e^{i(\phi_j - \phi_{j-1})} \} \cdot I_{j-1,j}(0) I_{j,j}(0) \quad (16) \\
 + 2 \operatorname{Re} \{ D_{j,m}^{\pm} \cdot D_{j+1,m}^{\pm} e^{i(\phi_j - \phi_{j+1})} \} \cdot I_{j+1,j}(0) I_{j,j}(0) \\
 \left. + 2 \operatorname{Re} \{ D_{j-1,m}^{\pm} \cdot D_{j+1,m}^{\pm} e^{i(\phi_{j-1} - \phi_{j+1})} \} \cdot I_{j-1,j}(0) I_{j+1,j}(0) \right)$$

9 When calculating the correspondent SXR, it can be observed that, in DPSK, the SXR for arbitrary
 10 phase of single ended differential detection is low bounded by:

$$11 \quad \operatorname{Min}(SXR_{diff}) = \frac{|I_{j,j}(0)|^2}{|I_{j-1,j}(0)|^2 + |I_{j+1,j}(0)|^2 + 2|I_{j-1,j}(0)I_{j,j}(0)\cos(\phi_j - \phi_{j-1})| + 2|I_{j+1,j}(0)I_{j,j}(0)\cos(\phi_j - \phi_{j+1})| + 2|I_{j-1,j}(0)I_{j+1,j}(0)\cos(\phi_{j-1} - \phi_{j+1})|} \quad (17)$$

13 In the case of $\phi_j = \phi_0 + j\pi/2$, similar to direct detection, the signal-crosstalk beating terms are
 14 eliminated and therefore the low bounded SXR can be obtained from:

$$15 \quad \operatorname{Min}(SXR_{diff}) \Big|_{\phi_j = \phi_0 + j\pi/2} = \frac{|I_{j,j}(0)|^2}{|I_{j-1,j}(0)|^2 + |I_{j+1,j}(0)|^2 + 2|I_{j+1,j}(0)I_{j-1,j}(0)|} = 2 \times \operatorname{Min}(SXR_{dd}) \Big|_{\phi_j = \phi_0 + j\pi/2} \quad (18)$$

16 In the CoWDM odd/even modulated configuration using only 2 modulators, i.e. $D_{j-1,m} = D_{j+1,m}$, the
 17 crosstalk terms in Eq. (16) can also be fully eliminated, which will be demonstrated numerically and
 18 experimentally in the next sections.

19

20 **2.3 Coherent Detection**

21 In this case, for simplicity, the polarization of the input CoWDM is assumed to be controlled to
 22 match that of the local oscillator. Assuming the use of a 90° optical hybrid with balanced
 23 photodiodes for the j^{th} channel, the sampled value for the in-phase and quadrature components for
 24 the m^{th} bit is given by:

$$25 \quad \left. \begin{aligned} V_{j,in-phase}(mT) &\propto \operatorname{Re} \left\{ D_{j,m} I_{j,j}(0) e^{i\phi_j - i\phi_0} + \sum_{n \neq m} D_{j,n} I_{j,j}((m-n)T) e^{i\phi_j - i\phi_0} + \sum_{k \neq j} \sum_n D_{k,n} I_{k,j}((m-n)T) e^{i\phi_k - i\phi_0} \right\} \\ V_{j,quadrature}(mT) &\propto \operatorname{Im} \left\{ D_{j,m} I_{j,j}(0) e^{i\phi_j - i\phi_0} + \sum_{n \neq m} D_{j,n} I_{j,j}((m-n)T) e^{i\phi_j - i\phi_0} + \sum_{k \neq j} \sum_n D_{k,n} I_{k,j}((m-n)T) e^{i\phi_k - i\phi_0} \right\} \end{aligned} \right\} \quad (20)$$

26 Again, the ISI is neglected, and it is assumed that the crosstalk comes only from the adjacent
 27 subcarriers $D_{j-1,m}$ and $D_{j+1,m}$:

$$28 \quad \left. \begin{aligned} V_{j,in-phase}(mT) &\propto \operatorname{Re} \left\{ D_{j,m} I_{j,j}(0) e^{i\phi_j - i\phi_0} + D_{j-1,m} I_{j-1,j}(0) e^{i\phi_{j-1} - i\phi_0} + D_{j+1,m} I_{j+1,j}(0) e^{i\phi_{j+1} - i\phi_0} \right\} \\ V_{j,quadrature}(mT) &\propto \operatorname{Im} \left\{ D_{j,m} I_{j,j}(0) e^{i\phi_j - i\phi_0} + D_{j-1,m} I_{j-1,j}(0) e^{i\phi_{j-1} - i\phi_0} + D_{j+1,m} I_{j+1,j}(0) e^{i\phi_{j+1} - i\phi_0} \right\} \end{aligned} \right\} \quad (21)$$

29 In back-to-back PSK, or any other single quadrature modulation format, $D_{k,n}$ and $I_{k,n}(t)$ may be
 30 considered to be real. Therefore, the in-phase component can be expressed as:

$$V_{j,in-phase}(mT) \propto D_{j,m} I_{j,j}(0) \cos(\phi_j - \phi_{lo}) + D_{j-1,m} I_{j-1,j}(0) \cos(\phi_{j-1} - \phi_{lo}) + D_{j+1,m} I_{j+1,j}(0) \cos(\phi_{j+1} - \phi_{lo}) \quad (22)$$

2 and the quadrature component is the same, except for the $\cos()$ terms which are replaced with $\sin()$.

3 Therefore, the low bounded SXR is:

$$Min(SXR_{CD}) = \frac{|I_{j,j}(0)|}{|I_{j-1,j}(0) \cos(\phi_j - \phi_{j-1})| + |I_{j+1,j}(0) \cos(\phi_j - \phi_{j+1})|} \quad (23)$$

5 In the case of $\phi_j = \phi_0 + j\pi/2$, and for a single quadrature signal, Eq. (21) shows that the crosstalk is
6 orthogonal to the signal field, and, consequently, results in an infinite SXR. The impact of the
7 crosstalk is shown in Figure 2 for two particular phase relationships between the subcarriers:
8 $\phi_j = \phi_0 + j\pi/2$ and $\phi_j = \phi_0$. The length of the blue arrows represents the crosstalk level which is
9 determined by the filter responses $I_{k,j}(0)$, whilst the position along the blue arrow is determined by
10 the data carried by the interfering subcarriers. Clearly, when $\phi_j = \phi_0 + j\pi/2$, it is possible to arrange for
11 the crosstalk to fall orthogonally to the signal, and, consequently, eliminating any impact from the
12 crosstalk.

13 In general, a summary of the derivations from sections 2.1 to 2.3 is represented in Figure 3. It
14 shows the variation in the SXR for systems where the crosstalk amplitude of the nearest neighbors,
15 at the sampling instant of the targeted channel j , is 1% of the signal level on that sample
16 $I_{j\pm 1,j}(0) = 0.01 \times I_{j,j}(0)$, and the filters are chirp free.

17 The figure clearly shows that the SXR is optimal when the phase difference between adjacent sub-
18 channels is $\pi/2$ for all cases. Furthermore, under optimized phase, coherent detection results in a
19 higher SXR, indicating its advantages when compared to other detection methods. However, this
20 simple analytical treatment suggests that if residual crosstalk exists ($I_{kj}(mT) \neq 0$), the number of
21 independent modulated signal has a significant impact on the results.

22 3. Numerical Simulations

23 3.1 Simulations for a 5-subcarrier CoWDM system

24 In section 2, we assumed, for clarity, that the filters were ISI free. However, this is unlikely to be the
25 case for the $(j+1)^{th}$ channel passing through the j^{th} filter. Numerical simulations were performed in to
26 verify the general trends of the analytical approach, and to examine the impact of ISI.

27 Figure 4 shows the simulation model of the CoWDM system used in this paper. The first stage of
28 the CoWDM system is the comb generator/laser source which is used to generate the equally
29 spaced sub-carriers at a frequency equal to the symbol rate of a single channel. In this case, five
30 coherent optical subcarriers with equal intensities and phases were produced using a comb
31 generator. The subcarrier spacing was 10GHz, equal to the data rate of each subcarrier, which
32 were modulated by uncorrelated 10Gbit/s data streams with temporally aligned eye crossings for
33 ASK, DPSK and BPSK modulation formats. The data streams consisted of $2^{11}-1$ pseudo-random
34 binary sequences (PRBS) repeated 5 times (10,235 bits) and delayed by 6, 70, 101, 125 and 205
35 bits in order to obtain the uncorrelated bit sequences. Ten '0' bits and eleven '0' bits were added
36 before and after each data train to simplify the boundary conditions. The electrical '1' bits were
37 raised-cosine shaped with a roll-off coefficient of 0.4 and were simulated with 40 samples per bit.
38 The modulated subcarriers were phase shifted by $k \times \Delta\phi$ ($k=0, \dots, 4$) before they were passively
39 combined. Note that, although only one variable $\Delta\phi$ was used to investigate the influence of phase
40 difference between subcarriers, these phase shifts are expected to include the best and the worst
41 performance cases, as illustrated in Fig. 3.

42 At the receiver, the noise of the optical preamplifier was modeled as additive white Gaussian noise
43 with equal noise spectral power density for each polarization. We followed the conventional
44 CoWDM demultiplexing approach [9-13], which may also be viewed as a 1 tap discrete Fourier
45 transform (DFT) filter [2,6,7], in which the five subcarriers were demultiplexed by an asymmetric

1 Mach-Zehnder interferometer (AMZI), with 20GHz free spectral range (FSR) to separate the odd
2 and even subcarriers, followed by 3rd-order Gaussian-shaped optical band-pass filters (OBPFs).
3 The signals after the OBPFs had a power of -3dBm per subcarrier and were detected directly
4 (ASK), differentially (DPSK), or coherently (BPSK) using balanced detection. In coherent detection,
5 the signals and local oscillators were separated into two linear polarization components with
6 polarization beam splitters (PBSs), mixed by 90^o optical hybrids, and detected by balanced
7 detectors to extract the in-phase and quadrature components. The output powers of the local
8 oscillators were +10dBm, and their phases were assumed not to vary during the simulation, and
9 therefore electrical phase equalization was not required. The equivalent thermal noise spectral
10 power density of the detectors was 18pA/ $\sqrt{\text{Hz}}$. After optical-to-electrical conversion, the signals
11 were electrically amplified, filtered by a 15GHz 4th-order Bessel electrical filters (EFs), sampled,
12 and decoded by optimal threshold decoding. The simulation was iterated 10 times with different
13 random number seeds to give a total of 102,350 simulated bits. The performance was evaluated in
14 terms of the required normalized optical signal-to-noise ratio (OSNR) at the photodiode to achieve
15 a bit error rate (BER) of 5×10^{-4} by direct error counting. The simulated bit number produces a
16 confidence interval of [3×10^{-4} - 7.5×10^{-4}] for this BER with 99% certainty. The normalized OSNR
17 was defined by:

$$18 \quad \text{Normalized OSNR} = \frac{\text{Total Signal Power}}{5 \times \text{Noise Power in } 0.1nm} \quad (24)$$

19 Figure 5 shows the performance of the center (Ch3 - squares), inner (Ch2/Ch4 - triangles) and
20 outer subcarriers (Ch1/Ch5 - circles) against the bandwidth of the OBPF for (a) ASK, (b) DPSK,
21 and (c) BPSK, with a phase difference between subcarriers of $\pi/2$. It is clear from the figure that the
22 optimized filter bandwidths lie between 1.5 and 2.5 \times the baud rate (15 - 25GHz) for all cases. The
23 OBPF bandwidth should be selected to achieve not only a balance between inter-symbol
24 interference and inter subcarrier crosstalk, but also a balance between the crosstalk from the most
25 adjacent subcarrier, referred to herein as inner-neighbors, and that from the next nearest
26 subcarriers (or outer-neighbors). At the narrower bandwidth region (<15GHz), the crosstalk from
27 the inner-neighbors dominated. Consequently, Ch1/Ch5, which only had one inner-neighbor,
28 exhibited better performance than Ch2/Ch4 and Ch3, having two inner-neighbors. However, at the
29 wider bandwidth region (>25GHz), the crosstalk levels for the subcarriers with two outer-neighbors
30 increased significantly. Furthermore, at the optimum phase $\phi_j = \phi_0 + j\pi/2$, the influence of the inter-
31 neighbors was mitigated such that the crosstalk from the outer-neighbors dominated the system
32 performance. Consequently, Ch2/Ch4 had similar performance as Ch1/Ch5 because they only had
33 one outer-neighbor, and all were better than that of Ch3, which had two outer-neighbors.

34 In figure 6, the phases between the subcarriers were varied where, and the normalized OSNR
35 versus the phase $\Delta\phi$ for all five subcarriers (Ch1-5) was measured for the three modulation formats
36 (a) ASK, (b) DPSK and (c) BPSK.

37 The 3dB bandwidth of the OBPF, in this case, was around twice the bit rate (20GHz). As expected,
38 the performance variations of Ch1/Ch5 were less than that of the center subcarrier (Ch3) and
39 Ch2/Ch4, and the performance was optimal when the phase difference between adjacent sub-
40 channels was $\pm\pi/2$, where the residual crosstalk from the inner-neighbors was orthogonal to the
41 signal. On the other hand, when the signal-crosstalk beating was not mitigated ($\Delta\phi=0, \pi, 2\pi$), an
42 additional 3~5dB OSNR penalty was induced for Ch3.

44 3.2 Simulations for a 3-subcarrier CoWDM system

45 In order to enable direct comparison with the experimental results that will be discussed in section
46 4, and to demonstrate the impact of using only 2 modulators in an odd/even modulated
47 configuration, the simulations from 3.1 were performed, but in a 3-subcarrier DPSK CoWDM
48 system. Here two different scenarios were used: (i) with all optical subcarriers independently
49 modulated (independently modulated configuration), and (ii) where only 2 modulators were used
50 (odd/even modulated configuration), i.e., the outer subcarriers were modulated with the same data.

1 In the simulations with the independently modulated configuration, 3 optical subcarriers with the
2 same intensity and phase were generated by an optical comb generator, and modulated by DPSK
3 data individually. The bandwidth of the modulator was set to be 13GHz. The simulated data
4 parameters, including the PRBS length and boundary conditions, were the same as section 3.1.
5 Additional phase shifts ($0, \Delta\phi, 0$) were placed on each subcarrier to investigate the phase
6 influence. At the receiver, the signals were demultiplexed by a 0.3nm Gaussian-shaped filter, an
7 AMZI with FSR of 20GHz and 20dB extinction ratio, and a 3rd-order Gaussian-shaped bandwidth-
8 tunable optical filter. The received optical power at the receiver was 0dBm and a 7GHz Bessel
9 electrical filter was also deployed at the receiver. The performance for the independently
10 modulated configuration as a function of filter bandwidth is illustrated in Figure 7(a), where circles,
11 triangles, and squares represent the left (Ch1), center (Ch2), and right (Ch3) subcarriers
12 respectively.

13 The optimal bandwidth of the outer (Ch1 and Ch3) subcarriers was 25GHz, and the overall
14 bandwidth, including the 0.3nm filter, was around 20GHz, similar to that in the five-subcarrier case.
15 However, in contrast, the optimal filter bandwidth for the center subcarrier was between 30-50GHz,
16 wider than that of the neighboring subcarriers (Left/Right) at optimized phases. This is because
17 only 3 subcarriers were used, such that no outer-neighbors existed, which would cause penalties
18 as the filter bandwidth increased. Figure 7(b) shows the required normalized OSNR versus the
19 phase for the independently modulated configuration. The bandwidth of the tunable OBPF was
20 26GHz for the outer subcarriers (Left/Right) and 45GHz for center one. The figure also shows that
21 $\pi/2$ was the optimal phase to achieve the best performance for this configuration, and the
22 performance of the center subcarrier was more dependent on the relative phase. On the other
23 hand, in order to investigate the effect of using the same data patterns for the adjacent neighboring
24 subcarriers on the performance, we also simulate a 3-subcarrier CoWDM system with odd/even
25 modulated configuration. In this simulation, 3 optical subcarriers were separated into even and odd
26 paths by an AMZI disinterleaver, and the relative phase of the center subcarrier was controlled with
27 respect to the outer channels by a phase shift of $\Delta\phi$. The demultiplexing setup was the same as
28 that of the independently modulated configuration. Figure 7(c) shows that, when compared to Fig.
29 7(a), the overall performances for all subcarriers were improved by using the odd/even modulated
30 configuration, which we attribute primarily due to the loss of crosstalk from non-identical inner-
31 neighbors as identified in section 2. Another typical feature of the figure is that the required OSNR
32 decreased below the value for an isolated sub-carrier with the OBPF bandwidth. This is attributed
33 to the fact that both subcarriers carried the same data, and a wider bandwidth increased the signal
34 power instead of crosstalk. Fig. 7(d) depicts the performance versus the phase. The bandwidth of
35 the OBPF was 26GHz for the outer subcarriers (Left/Right) and 45GHz for center subcarrier, for a
36 fair comparison with Fig. 7(b). The figure shows that Ch1 and Ch3 exhibited an improved
37 performance and a similar profile as those in Fig. 7(b). However, the profile of Ch1 was somewhat
38 different. Due to a π phase shift, introduced between the Left and Right optical subcarriers when
39 they were disinterleaved by the AMZI, and to the same data patterns between these two
40 subcarriers, any crosstalk from $D_{j-1,m}$ and $D_{j+1,m}$ to $D_{j,m}$ would be canceled. In this case, the influence
41 from other crosstalk terms, excluding $D_{j\pm 1,m}$ which were not included in section 2, became visible.
42 These terms resulted in an optimized $\Delta\phi$ of 0 and π , instead of $\pi/2$. The contributions of these
43 crosstalk terms were present, but were small, with an OSNR fluctuation of less than 0.4dB.

44 4. Experiments

45 In section 2 it was observed that the use of only two modulators in an odd/even configuration
46 neglects penalties arising from different data symbols on the two nearest interfering channels. This
47 was verified by the numerical simulations in section 3. To experimentally verify this, independent
48 modulation of a minimum of three subcarriers is required. A general CoWDM schematic is shown in
49 Figure 4, where a single laser source is used as a seed to a comb generator, whose output is
50 typically followed by an amplifier, in order to maintain an adequate OSNR, and a demultiplexer to
51 separate each subcarrier prior to modulation. An alternative method for subcarrier generation and

1 data encoding is the use of injection locked lasers (CW or tunable) [11-13, 22-23], which enables
2 each laser to be phase locked to one of the selected comb lines, avoiding excess loss of additional
3 components, and providing high extinction ratio and power efficiency. In this section, we present
4 the experimental investigation of a 3-subcarrier 32Gbit/s DPSK CoWDM system in the two
5 configurations used in the simulations in section (3.2); i.e using three independent modulators (4.1)
6 (independently modulated subcarriers), based on injection locked lasers, and secondly using a
7 more traditional scheme of odd/even modulated subcarriers (4.2) using a standard comb generator.
8 These two experiments show the impact of the additional crosstalk terms that appear when more
9 than two data encoding streams are used. Note that, because in a practical experimental
10 realization the different subcarriers actually go through different paths, and unless an integrated
11 device is used, random environment changes will cause each separate path to suffer from random
12 length change resulting in random phase variations. In order to compensate for the phase
13 variations, a phase stabilization circuit is required [10]. But, in this paper, since the temperature
14 was kept fairly stable, the phase adjustments were made manually.

15 16 **4.1. Independently modulated 3-subcarrier DPSK CoWDM system**

17 The experimental setup for the independently modulated 3-subcarrier DPSK CoWDM system is
18 shown in Figure 8 (left). The output of a fiber laser source (centered at 1553.175nm) was split as
19 follows: 10% was used for the center subcarrier, and the remaining 90% was used to generate a 3-
20 line comb signal spaced at 10.664GHz using a single Mach-Zehnder modulator (MZM). The 3-line
21 comb signal then was launched to a circulator and a splitter (all polarization maintaining) in order to
22 injection lock two DFB lasers, corresponding to the left and right spectral lines from the center
23 subcarrier, resulting in left and right subcarriers spaced by 21.328GHz. The 21.328GHz beat signal
24 between the left and right subcarriers was observed at the third output of the circulator, as shown in
25 Figure 8 (bottom-left), confirming that both lasers were successfully injection locked in frequency
26 and phase. The use of injection locked lasers enables the power of the subcarriers to be equalized,
27 relaxing the power and flatness constraints imposed on the primary comb generator, and improving
28 the OSNR and power efficiency [11-12]. Each of the 3-subcarriers were independently DPSK
29 modulated by a 10.664Gbit/s electrical data stream with a pseudo random bit sequence (PRBS)
30 length of $2^{31}-1$. The data streams had a -10-bit and +7-bit delays for the left and right subcarriers
31 respectively. A piezo-electric fiber stretcher was inserted after the output of each injection locked
32 DFB laser in order to adjust the relative phases of the outer subcarriers to the center one. The 3
33 DPSK modulated subcarriers were then combined using a planar waveguide power combiner,
34 resulting in a 32 Gbit/s DPSK CoWDM signal as shown in figure 8 (right).

35 36 **4.2. Odd/even modulated 3-subcarrier DPSK CoWDM system**

37 For comparison with the setup in 4.1, the experimental setup from Figure 8 was manipulated in
38 order to achieve a 3-subcarrier DPSK CoWDM system with a conventional odd/even modulated
39 configuration, as shown in Figure 9.

40 A 3-line comb signal was generated from the same source used in the previous section (fiber laser
41 and MZM). A standard commercial MZM was modulated with less than V_{π} by a 10.664GHz clock
42 signal to generate two side-bands, such that any additional harmonics were suppressed by more
43 than 25dB. The side-bands were separated from the central carrier by the clock frequency
44 (10.664GHz) and the dc-bias was used to match the amplitude of these side-bands to the central
45 carrier with a flatness of less than 0.5dB. This signal was amplified and launched to cascaded dis-
46 interleavers based on AMZIs (Kylia), with free spectral range (FSR) of 21.33GHz, to separate the
47 odd (center) and even (left and right) subcarriers. Cascading the AMZIs increases the extinction
48 ratio from around 21dB, where coherent crosstalk would degrade the signal, to >40dB, where such
49 crosstalk may be neglected. The additional loss associated with such cascaded filtering would be
50 avoided by the use of injection locked lasers, as per section 4.1. Two de-correlated 10.664Gbit/s
51 electrical data streams (with 26-bit differential delay) and a PRBS length of $2^{31}-1$ were used to drive
52 the two DPSK modulators to modulate the odd and even subcarriers with different data before

1 optically combining them resulting in a 32Gbit/s DPSK CoWDM signal. Also piezo-electric fiber
2 stretchers were inserted in the optical paths to adjust the phase between the odd and even
3 subcarriers.

4 4.3. Receiver

5 For both transmitter cases, the receiver configuration used is shown in Figure 10. The pre-amplified
6 scheme used a variable optical attenuator (VOA) to vary the input power to the receiver, followed
7 by a low noise pre-amplifier (EDFA 1). An optical 0.3nm-bandwidth tunable band-pass filter was
8 used to select the subcarrier under test, followed by an AMZI (Kylia), with an FSR of 21.33GHz, to
9 suppress the adjacent subcarriers. A second amplifier (EDFA 2) was used to boost the signal
10 power to the remaining receiver, comprising of a bandwidth adjustable filter, which was optimized
11 for each received subcarrier (50GHz for the center and 30GHz for the outer subcarriers), and a
12 DPSK demodulator (1-bit delay AMZI). The demodulated signal was detected using a balanced
13 photodiode and amplified using a limiting differential amplifier, and then launched to the error
14 detector (ED) and high speed oscilloscope (Osc.).
15

16 17 18 19 4.4. Experimental results

20 The performance of both CoWDM transmitter implementations was evaluated by measuring the
21 BER waterfall curves of the 3 received CoWDM subcarriers. The results shown in Figure 11 takes
22 into account adjustments of the relative phases for optimal performance (lowest BER), and
23 detuning them for a degraded BER.

24 The average receiver sensitivity (total received power to achieve an average BER of 10^{-9} for the 3-
25 subcarriers was -33.2dBm and -34.5dBm for the independently modulated and odd/even
26 modulated configurations respectively, showing a clear 1.3dB improvement when odd/even
27 subcarriers were used. When the relative phases are detuned, there is a negligible penalty for the
28 outer subcarriers, with a larger deterioration for the center one. Moreover, for the independently
29 modulated configuration, a BER floor at around 10^{-4} is evident for the center subcarrier. This error
30 floor, at a detuned phase, and the enhanced receiver sensitivity, at the optimum phase, are due to
31 the fact that the center subcarrier is more affected from the interference of the neighboring
32 subcarriers carrying different data patterns, and in particular when the neighboring subcarriers
33 carry inverted data symbols. This observation also agrees with the simulation results shown in
34 Figure 7 (b and d). Such interference could be reduced, or even eliminated, by using an improved
35 filter, closer to a matched or ideal filter, at the receiver. The demodulated eye diagrams for the
36 subcarriers for both configurations are also shown in Figure 11 (top). It should be noted that, for the
37 odd/even modulated case, a strong beating signal is observed for the center subcarrier as both
38 neighbor subcarriers carry the same data patterns which is not the case for the center channel in
39 the independently modulated configuration. The BER for the center subcarrier, in an odd/even
40 modulated configuration, was also measured when varying the relative phase of the outer
41 subcarriers, as shown in Figure 12 (left). It clearly shows the periodicity with phase ϕ , as predicted
42 analytically and numerically (Figures 3 and 7 respectively). Figure 12 (right) shows a comparison in
43 terms of numerically simulated received OSNR penalty (for a 3-subcarrier 30Gbit/s DPSK system)
44 and experimentally observed received power penalty (for a 3-subcarrier 32Gbit/s DPSK system)
45 between best and worse phase performances required to obtain a BER of 5×10^{-4} for both
46 independently modulated and odd/even modulated configurations. In all cases, it clearly shows that
47 the center subcarrier will always be further deteriorated, as it has the impact of both outer
48 subcarriers. As predicted, the odd/even modulated configuration gives lower penalties, as some of
49 the analytical terms are null. The difference in the results obtained numerically and experimentally
50 could be due to non-ideal components used in the experimental setup.

5. Conclusions

We have presented analytical and numerical analyses which assesses the impact of the relative phase relationship between subcarriers on CoWDM systems, using direct detection for ASK, and differential/coherent detection for BPSK. These analyses were also verified experimentally using differential detection for DPSK signals. We have further demonstrated that the commonly used odd/even configuration may under-estimate the average receiver sensitivity penalty by 1.3dB when compared to practical implementations using an independently modulated configuration. However, in all cases, by controlling the relative phases between the sub-carriers the receiver sensitivity could be improved, avoiding large penalties and possible error floors. We conclude that low-cost optical receiver filters can therefore be used without sacrificing the performance, hence avoiding extra receiver complexity, and enabling a practical implementation of CoWDM.

6. Acknowledgment

This material is based upon work supported by Science Foundation Ireland under Grants 06/IN/1969 and 03/CE3/1405, and which received funding from the European Communities Seventh Framework Program FP/2007-2013 under grant agreement 224547 (PHASORS).

References

- [1] R. E. Mosier, R. G. Clabaugh, "Kineplex, A Bandwidth-Efficient Binary Transmission System", *AIEE Transactions*, vol. 76, pp. 723-728, 1958.
- [2] H. Sanjoh, E. Yamada, and Y. Yoshikuni, "Optical orthogonal frequency division multiplexing using frequency/time domain filtering for high spectral efficiency up to 1bit/s/Hz", *in Proc. OFC*, 2002, ThD1.
- [3] K. Yonenaga, F. Inuzuka, S. Yamamoto, H. Takara, B. Kozicki, T. Yoshimatsu, A. Takada, and M. Jinno, "Bit-Rate-Flexible All-Optical OFDM Transceiver Using Variable Multi-Carrier Source and DQPSK/DPSK Mixed Multiplexing", *in Proc. OFC*, 2009, OWM1.
- [4] A. Sano, H. Masuda, E. Yoshida, T. Kobayashi, E. Yamada, Y. Miyamoto, F. Inuzuka, Y. Hibino, Y. Takatori, K. Hagimoto, T. Yamada, and Y. Sakamaki, "30x100 Gb/s all-optical OFDM transmission over 1300 km SMF with 10 ROADM nodes", *in Proc. ECOC*, 2007, PD1.7.
- [5] S. Chandrasekhar, X. Liu, B. Zhu, and D.W. Peckham, "Transmission of a 1.2-Tb/s 24-Carrier No-Guard-Interval Coherent OFDM Superchannel over 7200-km of Ultra-Large-Area Fiber", *in Proc. ECOC*, 2009, PD2.6.
- [6] D. Hillerkuss, et al., "Simple all-optical FFT scheme enabling Tbit/s real-time signal processing", *Opt. Express*, vol. 18, pp. 9324-9340, 2010.
- [7] K. Takiguchi, et al., "Integrated-optic eight-channel OFDM demultiplexer and its demonstration with 160 Gbit/s signal reception", *Electron. Lett.*, vol. 46, no. 8, pp. 575-576, 2010.
- [8] H. Chen, et al., "All-optical sampling orthogonal frequency-division multiplexing scheme for high-speed transmission system", *J. Lightwave Technol.*, vol. 27, no. 21, pp. 4848-4854, 2009.
- [9] A.D. Ellis and F.C.G. Gunning, "Spectral Density Enhancement Using Coherent WDM", *Photon. Technol. Lett.*, vol. 17, no. 2, pp. 504-506, 2005.
- [10] F.C.G. Gunning, T. Healy, X. Yang, and A.D. Ellis, "0.6Tbit/s Capacity and 2bit/s/Hz Spectral Efficiency at 42.6Gsymbol/s Using a Single DFB Laser with NRZ Coherent WDM and Polarisation Multiplexing", *in Proc. CLEO-Europe*, 2007, C18-5-FRI.
- [11] S.K. Ibrahim, A.D. Ellis, F.C.G. Gunning, J. Zhao, P. Frascella, F. H. Peters, "Practical Implementation of Coherent WDM", *in Proc. IEEE Phot. Soc. Meeting*, 2009, Invited paper ThM1
- [12] S.K. Ibrahim, A.D. Ellis, F.C.G. Gunning, and F.H. Peters, "Demonstration of CoWDM Using a DPSK Modulator Array with Injection-locked Lasers", *Electron. Lett.*, vol. 46, no. 2, 2010.
- [13] S.K. Ibrahim, F.C.G. Gunning, and A.D. Ellis, "Performance Evaluation and Comparison of DPSK CoWDM Systems based on Odd/Even and Array Configurations", *in Proc. CLEO*, 2010, CThC3.
- [14] A. J. Lowery, L. Du, and J. Armstrong, "Orthogonal Frequency Division Multiplexing for Adaptive Dispersion Compensation in Long Haul WDM Systems", *in Proc. NFOEC*, 2006, PDP39.
- [15] B.J.C. Schmidt, A. James Lowery and J. Armstrong, "Experimental Demonstrations of 20 Gbit/s Direct-Detection Optical OFDM and 12 Gbit/s with a colorless transmitter", *in Proc. OFC*, 2007, PDP18
- [16] A. Sano, E. Yamada, H. Masuda, E. Yamazaki, T. Kobayashi, E. Yoshida, Y. Miyamoto, R. Kudo, K. Ishihara, and Y. Takatori, "No-Guard-Interval Coherent Optical OFDM for 100-Gb/s Long-Haul WDM Transmission", *J. Lightwave Technol.*, vol. 27, pp. 3705, 2009.

- 1 [17] W. Shieh, H. Bao, and Y. Tang, "Coherent Optical OFDM: Theory and Design", *Opt. Express*, vol. 16, no.
2 2, pp. 841-859, 2008.
- 3 [18] W. Shieh, Q. Yang, and Y. Ma, "107 Gb/s coherent optical OFDM transmission over 1000-km SSMF fiber
4 using orthogonal band multiplexing", *Opt. Express*, vol. 16, pp. 6378, 2008.
- 5 [19] S.L. Jansen, I. Morita, T.C. W. Schenk, and H. Tanaka, "121.9-Gb/s PDM-OFDM Transmission With 2-
6 b/s/Hz Spectral Efficiency Over 1000 km of SSMF", *J. Lightwave Technol.*, vol. 27, pp. 177, 2009.
- 7 [20] Jian Zhao, Andrew D. Ellis, "Electronic Signal Processing for Crosstalk- and ISI-Free Operation in All-
8 Optical OFDM", in *Proc. ECOC*, 2010, Accepted for publication
- 9 [21] G. Gavioli, E. Torrenco, G. Bosco, A. Carena, V. Curri, V. Miot, P. Poggiolini, M. Belmonte, F. Forghieri, C.
10 Muzio, S. Piciaccia, A. Brinciotti, A. La Porta, C. Lezzi, S. Savory, S. Abrate, "Investigation of the Impact
11 of Ultra-Narrow Carrier Spacing on the Transmission of a 10-Carrier 1Tb/s Superchannel", in *Proc. OFC*,
12 2010, OThD3
- 13 [22] S. K. Mondal, B. Roycroft, P. Lambkin, F. Peters, B. Corbett, P. Townsend, and A. Ellis, "A
14 Multiwavelength Low-Power Wavelength-Locked Slotted Fabry-Pérot Laser Source for WDM
15 Applications", *Photon. Technol. Lett.*, vol.19, pp. 744, 2007.
- 16 [23] B. Cai, D. Wake, and A.J. Seeds, "Microwave frequency synthesis using injection locked laser comb line
17 selection", in *Proc. IEEE LEOS Summer Top. Meet. RF Optoelectronics*, 1995, WD213-14.
- 18

1 Figure Captions

2
3 **Figure 1.** General schematic of a CoWDM system.

4
5 **Figure 2.** Constellation map of PSK with crosstalk with different subcarrier phase relationships.

6
7 **Figure 3.** Variation in the SXR as a function of the relative phase of the two nearest neighbour sub-
8 channels for (a) direct detected ASK signal, (b) differentially detected BPSK signal, and (c)
9 coherent detected BPSK signal with the filter performance characterized by $I_{j\pm 1,j}(0)=0.01 \times I_{j,j}(0)$
10 (Dotted red line shows the projection for the phase relationship ($\phi_{j-1}=0, \phi_j, \phi_{j+1}=0$)).

11
12 **Figure 4.** Simulation setup of a 5-subcarrier CoWDM system.

13
14 **Figure 5.** Performance of Ch1-5 versus the bandwidth of the OBPF for (a) ASK, (b) DPSK, and (c)
15 BPSK modulation formats (Ch1/Ch5: red circles; Ch2/Ch4: blue triangles; Ch3: green squares).

16
17 **Figure 6.** Normalized OSNR versus the phase $\Delta\phi$ for Ch1-5 when the modulation format is (a)
18 ASK, (b) DPSK, and (c) BPSK (Ch1/Ch5: red circles; Ch2/Ch4: blue triangles; Ch3: green squares).

19
20 **Figure 7.** 3-subcarrier DPSK CoWDM system performance as a function of the OBPF bandwidth
21 (left - (a), (c)) and the phase $\Delta\phi$ (right - (b), (d)) for independently mod. configuration (top) and
22 odd/even mod. configuration (bottom) (Ch1: red circles; Ch2: blue triangles; Ch3: green squares).

23
24 **Figure 8.** Experimental setup for independently mod. 32Gbit/s DPSK CoWDM Tx (left), including
25 beat signal between the three subcarriers (bottom-left). Spectrum of the 3 individual 10.664Gb/s
26 DPSK subcarriers (top-right) prior to power combiner, and CoWDM spectrum (bottom-right).

27
28 **Figure 9.** Experimental setup for 32Gbit/s DPSK CoWDM in an odd/even modulated configuration.

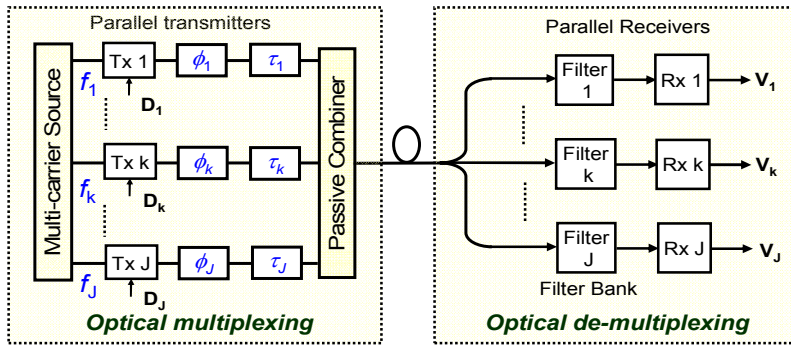
29
30 **Figure 10.** Experimental setup for a 32Gbit/s DPSK CoWDM Receiver.

31
32 **Figure 11.** 32 Gbit/s DPSK CoWDM for optimal and detuned relative phases for odd/even
33 modulated (left) and independently modulated (right) transmitter configurations with corresponding
34 demodulated eye diagrams (top).

35
36 **Figure 12.** (Left) BER for the center subcarrier against the relative phase in an odd/even mod.
37 configuration. (Right) Ratio between best and worst phases performance for numerically simulated
38 (Sim) and experimentally implemented (Exp) 3-subcarrier 10Gbaud DPSK CoWDM system.

39
40

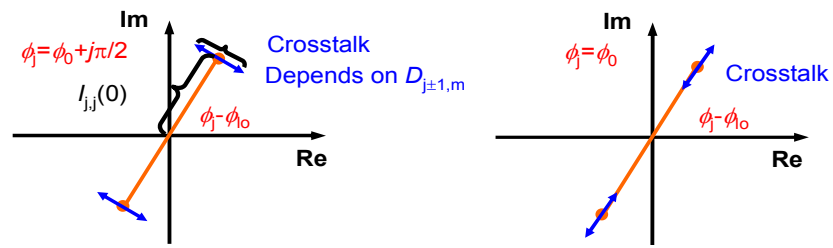
1
2



3
4
5
6
7
8
9
10

Figure 1

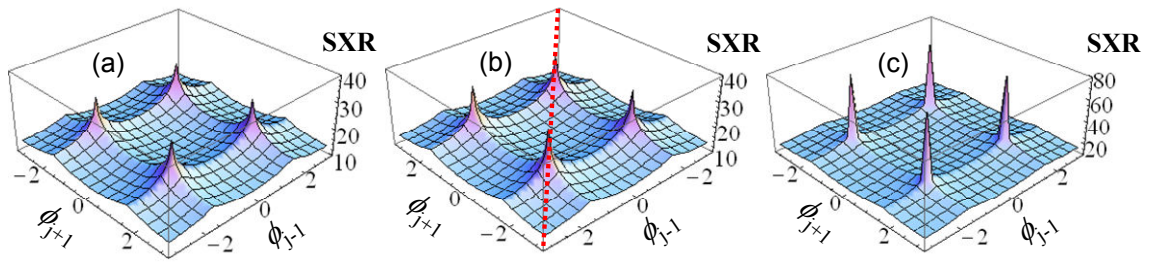
1
2



3
4
5
6

Figure 2

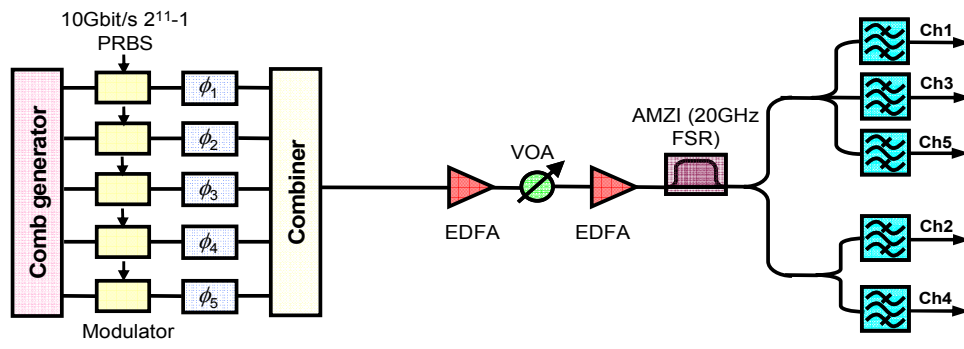
1
2



3
4
5
6

Figure 3

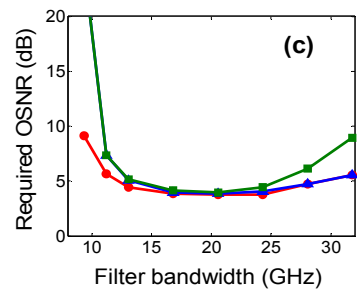
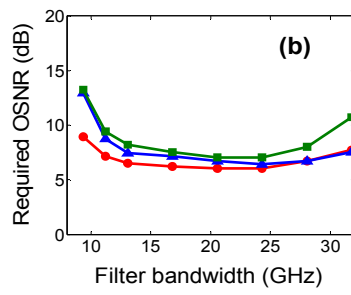
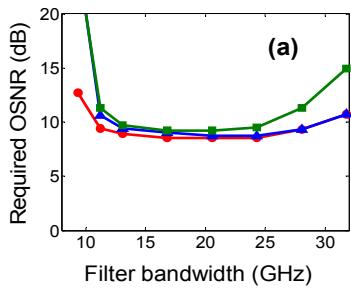
1
2



3
4
5
6

Figure 4

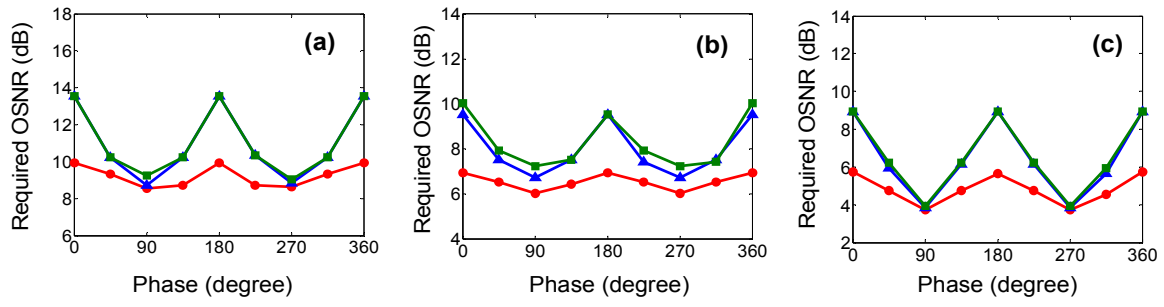
1
2



3
4
5
6

Figure 5

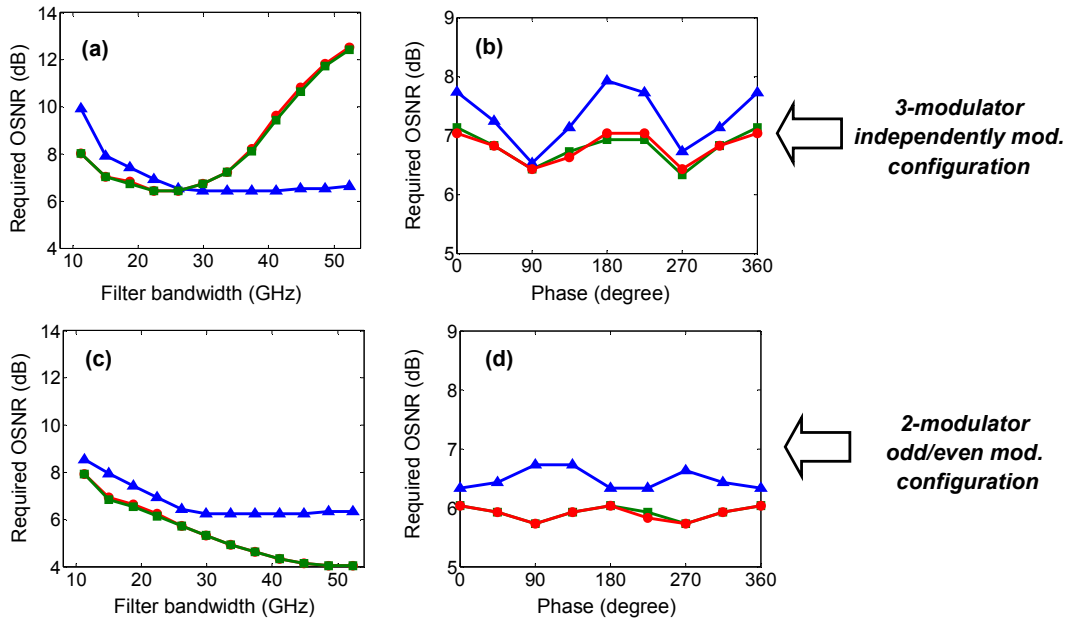
1
2



3
4
5
6

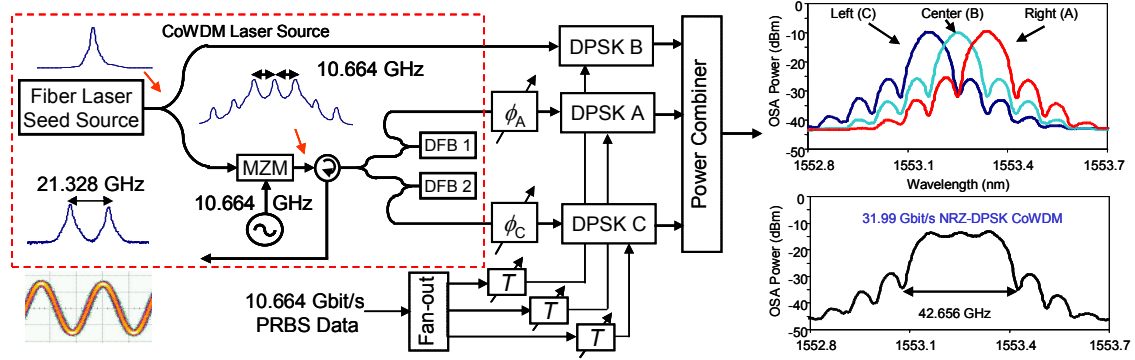
Figure 6

1
2



3
4
5
6 **Figure 7**

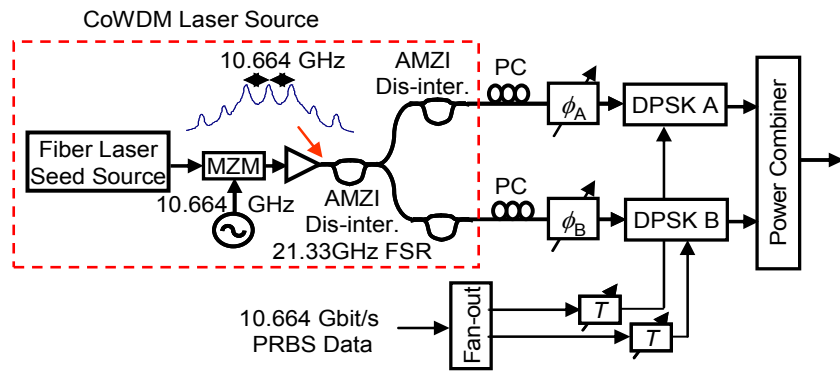
1
2



3
4
5
6
7
8

Figure 8

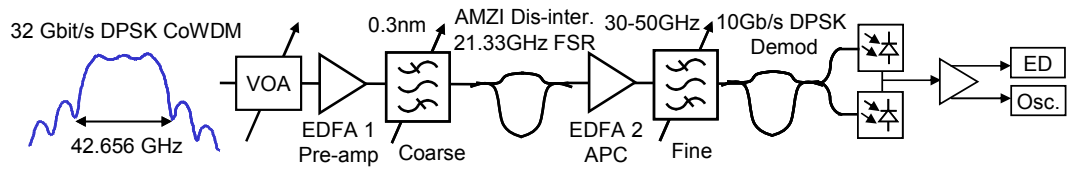
1
2



3
4
5
6
7

Figure 9

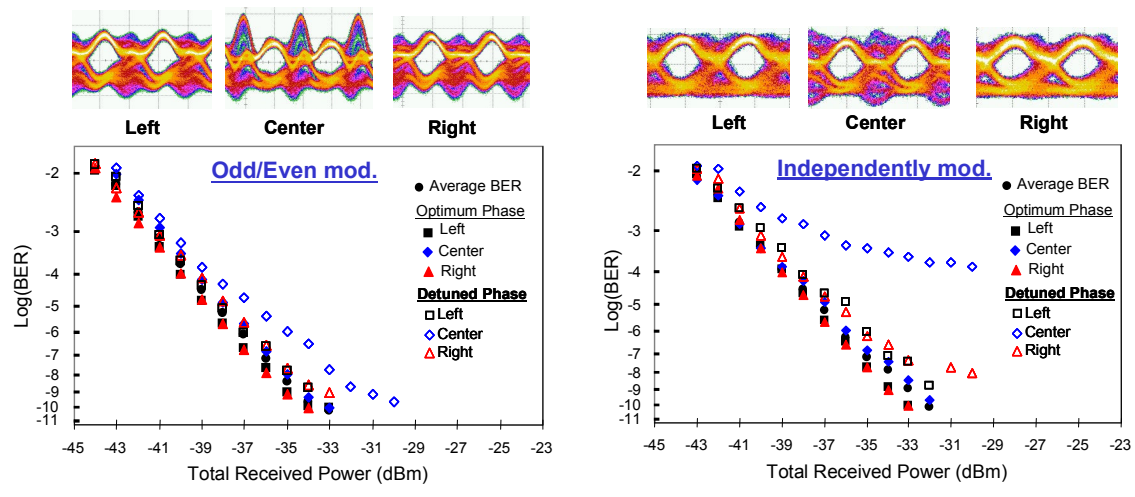
1
2



3
4
5
6
7

Figure 10

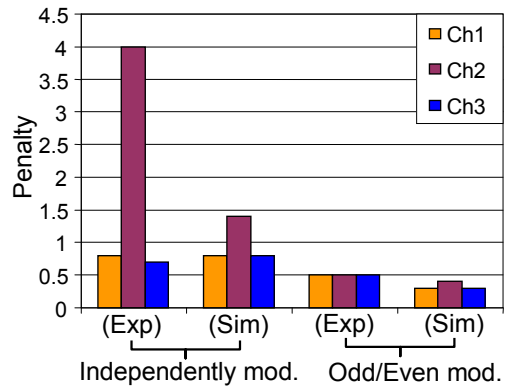
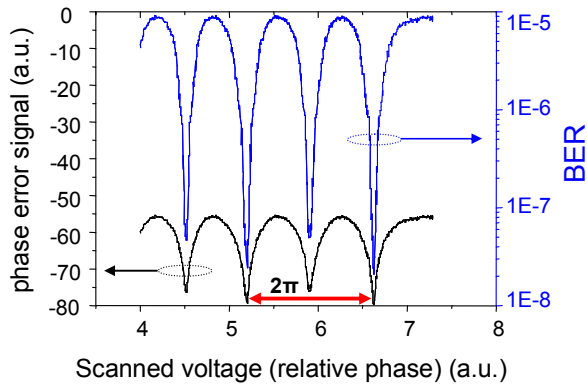
1
2



3
4
5
6
7

Figure 11

1
2



3
4
5
6
7
8

Figure 12